Transactions of A. Razmadze
Mathematical Institute
Vol. **176** (2022), issue 1, 57–72

CONSEQUENCE OF THERMOPHORESIS AND BROWNIAN MOTION ON THREE-DIMENSIONAL MAGNETOHYDRODYNAMIC CASSON NANO-FLUID FLOW WITH HEAT TRANSFER ANALYSIS

AAQIB MAJEED[1*], AHMAD ZEESHAN[2], SAJJAD ALI[3] AND FARZAN MAJEED NOORI[4]

Abstract. This paper investigates 3D chemically reactive magnetohydrodynamics (MHD) non-Newtonian Casson nano-fluid flow towards a stretchable porous surface. The effects of thermal radiation and Biot number on heat and mass transfer phenomena have also been examined. The well-known classical Navier-Stokes problem is modelled, and similarity functions are utilized to convert the nonlinear system of partial differential equations (PDEs) into ordinary differential equations (ODEs). Numerical illuminations are obtained with the help of MATLAB using a boundary value solver. The influence of dimensionless convergence flow parameters like nano-particle concentration, Lewis number, heat generation parameter, magnetic parameter, Casson fluid factor, Brownian motion parameter, chemical reaction rate, stretching ratio parameter, Prandtl number on velocity, temperature and concentration fields along with the heat transfer rate and friction factor and Sherwood numbers are beautifully tackled with the aid of tables and graphs. The essential outcomes indicate that enhancement is seen in concentration and temperature profiles by increasing the velocity slip parameter, whereas increment in stretching rate parameter decrement is perceived both in concentration and in temperature profiles.

1. Introduction

Nanotechnology has recently received a lot of attention, attracting many researchers and scientists due to its numerous applications in business and medicine, such as ceramics and drug delivery. Choi [2] was the forerunner in developing a magnificent and new process involving nanoparticles and the base fluid. For the sake of modern heat transfer fluids that are far more efficient from an energy-saving and environmental-cleaning standpoint, higher thermal conductivities are desirable. Nanofluid is a particular sort of medium for heat transfer consisting of nanoparticles of size about less than 100 nm, which are spread constantly and steadily in a fluid with a base like oil water-glycol and ethylene. The most frequently used nanoparticles are Al, Ti , Ag, Cu and their oxides to improve the nanoparticle thermal conductivity as well as convection and conduction coefficient taking, considering extra heat transference. Because of the linear stretching surface, Makinde et al. [14] investigated non-isothermal boundary layer nano-fluid fluid. The heat transfer properties for nano-fluid flow in the channel by considering two types of mixture models were stated by Sheikholeslami et al. [26]. Goodarzi et al. [7] recorded nano-fluids flow in a narrow cavity channel for laminar and turbulent cases. The flow for multiphase convection nano-fluid underneath the narrow transverse channel by using modified Buongiorno's model was proposed by Malvandi et al. [15].

The rheology of non-Newtonian fluids has got a lot of interest in the sciences and bioengineering because of their wide range of applications in food processing, metallurgy, drilling operations, the abstraction of basic oil from petroleum products, geophysics, and clay coating. Casson fluid has gained a lot of attention among non-Newtonian fluids because of its numerous uses in penetrating activities, nutrition control, and bio-engineering missions. Due to the boundless viscosity, Casson fluid is considered as diminishing fluid at a rate of zero. It yields stress beneath due to which no flow appears. The importance of non-Newtonian fluid, including conventional cushy stress, has directed many concepts of the present growth [4, 21]. In this discussion of non-Newtonian fluid, Casson fluid

2020 *Mathematics Subject Classification.* 76A05, 76D05, 76D10.

Key words and phrases. Brownian motion; Heat generation; Thermal radiation; Porous space; Casson nano-fluid; Numerically.

*Corresponding author.

has gained high importance in scientific and engineering areas. Casson presented his model for the viscoelastic fluid flow in 1995. Reddy [23] investigated a non-Newtonian unsteady fluid flow through a stretched plate. The non-Newtonian fluid flow under the influence of uniform temperature was studied by Khalid et al. [9]. Nazar et al. [20] and Ishak et al. [8] contributed to a stagnation point flow discussion over a stretching sheet. Khan et al. [11] implemented a power-law model for mixed convection flow and heat analysis of third-grade nano-fluid over a vertical heated surface. Ibrahim et al. [17] analyzed the MHD Casson nano-fluid flow through a stagnation point and analyzed that the viscosity of thermal boundary layers increased with increment in the slip factor.

Rashidi et al. [22] instigated that nano-fluid dynamic for an isothermal elongation sheet and special effects of transpiration by implementing the homotopy analysis method (HAM). Rahimi and Freidoonimehr [6] discussed the MHD nano-fluid flow past through a stretched surface by instigating partial slip effects. Tian et al. [27] established a scheme using a variant of Prandtl number model to improve the numerical model for the case of a super pressure fluid. Bukhari et al. [10] investigated MHD third-grade fluid flow over a stretching sheet under the influence of variable reactive index. Recently, Nadeem et al. [18] considered MHD boundary layer flow of Casson fluid past a linear stretching sheet. Esfe et al. [5] applied various intelligence artificial methods to estimate the viscosity of Tio_2/SAE 50 nano lubricants with Power-law models. The performance of hybrid nano-fluid with a specific discussion on thermo-physical, synthesis methodologies, histology, current position and some other salient features was discussed by Baber and Ali [1]. Manasrah et al. [16] engrossed in the development of constituents founded at the nanoparticles. Some recent investigations relate to the non-Newtonian fluid are discussed in [13,25]. Kilicman et al. [12] found ODEs of non-isothermal fluid transfer solution using a homotopy perturbation method. Nadeem et al. [19] analyzed radiative Jeffery fluid flow over an exponentially stretching sheet with prescribed boundary conditions.

From the above literature reviews, a lot of work is still present on the nano-fluid, so we expressed a strong desire to investigate the three-dimensional magnetohydrodynamic flow of Casson nano-fluid flow towards a stretching surface in the presence of thermophoresis, Brownian motion, and the impact of nanoparticle concentration. Numeric simulation with the bvp4c function in MATLAB was used to solve the resulting system of ODEs connected with the problem. Furthermore, the effects of non-dimensional flow parameters on velocity, temperature, concentration profiles, Nusselt number, skin friction, and Sherwood number are discussed using graphs and tables.

2. Mathematical Formulation of the Problem

In this section, we consider 3D incompressible Casson fluidic problem on the boundary layer segment using heat transfer and thermal radiation effect. The domain $z > 0$ occupies the flow, and the sheet has a fixed origin and is stretched in two directions. The $u = ax$ and $v = by$ are the respective velocities along with the axial and transverse directions. The geometrical model problem is demonstrated in Figure 1. Here, u, v and w indicate the velocity components in three lateral x, y and z directions. T_f and T_∞ indicate the surface and ambient temperatures. Furthermore, C_W and C_∞ represent nanoparticles concentration and the ambient concentration of the problem, respectively. By applying the boundary layer approximation, the governing equations are given as [17,18]:

$$\nabla.V = 0, \tag{1}$$

$$u\frac{\partial u}{\partial x} + v\frac{\partial u}{\partial y} + w\frac{\partial u}{\partial z} = \nu\Big(1 + \frac{1}{\beta}\Big)\Big(\frac{\partial^2 u}{\partial z^2}\Big) - \frac{\delta B^2}{\rho_f}u - \frac{\nu}{K}u, \tag{2}$$

$$u\frac{\partial v}{\partial x} + v\frac{\partial v}{\partial y} + w\frac{\partial v}{\partial z} = \nu\Big(1 + \frac{1}{\beta}\Big)\Big(\frac{\partial^2 v}{\partial z^2}\Big) - \frac{\delta B^2}{\rho_f}v - \frac{\nu}{K}v, \tag{3}$$

$$u\frac{\partial T}{\partial x} + v\frac{\partial T}{\partial y} + w\frac{\partial T}{\partial z} = \alpha\Big(1 + \frac{16\delta^* T_\infty^3}{\beta}\Big)\Big(\frac{\partial^2 T}{\partial z^2}\Big) + \tau\Big\{\frac{D_T}{T_\infty}\Big(\frac{\partial^2 T}{\partial z^2}\Big) + D_B\frac{\partial C}{\partial z}\frac{\partial T}{\partial z}\Big\} + \frac{Q^*}{(\rho C_p)_f}\left(T - T_\infty\right), \tag{4}$$

$$\frac{\partial C}{\partial x}+v\frac{\partial C}{\partial y}+w\frac{\partial C}{\partial z}=D_B\Big(\frac{\partial^2 C}{\partial z^2}\Big)-\delta\left(C-C_\infty\right)+\frac{D_T}{T_\infty}\frac{\partial^2 T}{\partial z^2}. \tag{5}$$

The corresponding boundary conditions are [18]:

$$\begin{gathered} u=U_w=ax,\quad u=axf'(\eta),\quad v=ayg'(\eta),\quad w=-\sqrt{\nu a}\left(f\left(\eta\right)+g\left(\eta\right)\right),\\ \phi\left(\eta\right)=\frac{C-C\infty}{C_w-C_\infty},\quad \theta\left(\eta\right)=\frac{T-T_\infty}{T_w-T_\infty}. \end{gathered} \tag{6}$$

The modelled equations (1), (2), (3), (4), (5), (6) and the associated boundary relation take the dimensionless form by using the similarity transformation

$$\Big(1+\frac{1}{\beta}\Big)f'''\left(\eta\right)+\left(f(\eta)+g(\eta)\right)f''\left(\eta\right)-\left(f'(\eta)\right)^2-\left(M^2+\lambda\right)f'\left(\eta\right)=0, \tag{7}$$

$$\Big(1+\frac{1}{\beta}\Big)g'''\left(\eta\right)+\left(f(\eta)+g(\eta)\right)g''\left(\eta\right)-\left(g'(\eta)\right)^2-\left(M^2+\lambda\right)g'\left(\eta\right)=0, \tag{8}$$

$$\Big(1+\frac{4}{3}N_r\Big)\theta''\left(\eta\right)+\Pr\left(f(\eta)+g(\eta)\right)\theta'\left(\eta\right)+Nb\theta'\left(\eta\right)\phi(\eta)+Nt\left(\theta'\left(\eta\right)\right)^2+\Pr Q\theta\left(\eta\right)=0, \tag{9}$$

$$\phi''\left(\eta\right)+Le\left(f(\eta)+g(\eta)\right)\phi'\left(\eta\right)+\frac{Nt}{Nb}\theta''(\eta)-Le\chi\phi(\eta)=0. \tag{10}$$

Here, the magnetic parameter is represented by $M=\frac{\sigma B_0^2}{\rho a}$, the Prandtle parameter is $Pr=\frac{\nu}{\alpha}$, the radiation parameter is $Nr=\frac{4\delta^* T_\infty^3}{kk^*}$, the Brownian parameter is $Nb=\frac{\tau D_B(C_w-C_\infty)}{\nu}$, the heat generation factor is $Q=\frac{Q^*}{(\alpha\rho C_p)}$, the chemical reaction factor is $\chi=\frac{\delta}{a}$, the porosity parameter is $\lambda=\frac{\alpha}{aK}$, c represents the ration of the velocities in x and y directions and the Lewis number is $L=\frac{\nu}{D_B}$.

The respective boundary conditions are:

$$\begin{gathered} f\left(\eta\right)=0,\quad f'\left(\eta\right)=1,\quad g\left(\eta\right),g'\left(\eta\right)=c,\quad \theta'(0)=-Bi\left(1+\theta(0)\right),\quad \phi(0)=1,\\ f'(\infty)=0,\quad g'(\infty)=0,\quad \theta(\infty)=0,\quad \phi(\infty)=0, \end{gathered}$$

where

$$Bi=\frac{h}{k}\sqrt{\frac{\nu}{k}},\quad C_{fx}=\frac{\tau_{wx}}{\frac{\rho f U_w^2}{2}},\quad C_{fy}=\frac{\tau_{wy}}{\frac{\rho f U_w^2}{2}},\quad N_{ux}=\frac{xq_w}{K_f(T_f-T_\infty)},\quad S_{hx}=\frac{xq_m}{D_B(C_w-C_\infty)}.$$

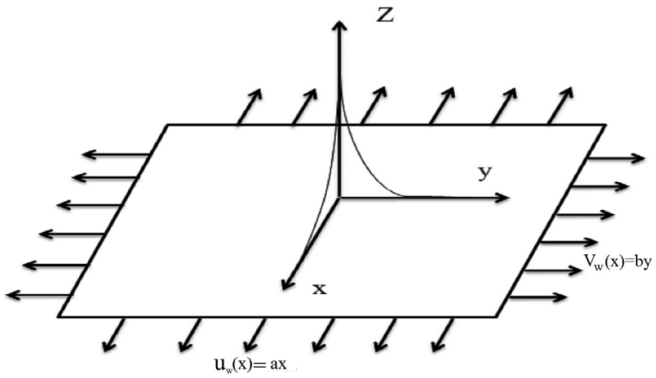

FIGURE 1. Physical sketch of the problem.

3. Solution Methodology

In the recent demonstration, a well-known sophisticated numerical scheme called boundary value problem solver bvp4c is employed to solve the system of highly nonlinear equations (7), (8), (9), (10) with the boundary condition (11). The domain $[0, \eta_\infty]$ is considered for the proposed problem. The value of the $\eta_\infty = 8$ has been chosen throughout the article. To get the first order ODEs system, we use the notation $y_1 = f, y_4 = g, y_7 = \theta, y_9 = \phi$.

$$
\begin{aligned}
y_1^{'} &= y_2 && y_1(0) = 0,\\
y_2^{'} &= y_3 && y_2(0) = 1,\\
y_3^{'} &= \tfrac{\beta}{1+\beta}\left[-y_1 y_3 - y_3 y_4 + y_2^2 + \left(M^2 + \lambda\right) y_2\right] - && y_3(0) = p,\\
y_4^{'} &= y_5 && y_4(0) = 0,\\
y_5^{'} &= y_6 && y_5(0) = c,\\
y_6^{'} &= \tfrac{\beta}{1+\beta}\left[-y_1 y_6 - y_4 y_6 + y_2^2 + \left(M^2 + \lambda\right) y_5\right] && y_6(0) = q,\\
y_7^{'} &= y_8 && y_7(0) = r,\\
y_8^{'} &= \tfrac{3}{3+4Nr}\left[-(y_1 + y_4)\Pr y_8 - Nb y_8 y_{10} - Nt y_8^2 - \Pr Q y_7\right] && y_8(0) = -Bi\left(1 - y_7(0)\right),\\
y_9^{'} &= y_{10} && y_9(0) = 1,\\
y_{10}^{'} &= -Le(y_1 + y_4) y_{10} - \tfrac{Nt}{Nb} y_8^{'} - Le\chi y_9 && y_{10}(0) = t.
\end{aligned}
$$

Here, p, q, r and t are the missing initial conditions.

4. Results and Discussions

In this section, we have analyzed the velocity profiles $f'(\eta)$ and $g'(\eta)$ for different physical parameters such as Casson fluidic parameter β, magnetic parameter M, porosity parameter λ, nanoparticle concentration C, thermophoresis parameter Nt, Lewis number Le, Brownian motion parameter Nb, radiation parameter Nr and chemical reaction factor χ. Table 1 validates that the present results of skin friction coefficients, which shows a superb accuracy with those achieved by Nadeem et al. [18] with the absence of both porosity parameter λ and Casson fluid parameter β. Table 2 shows the heat transfer rate increases by enhancing the value of the physical parameters Nb, Pr and Bi while quite diverse behavior is noted for Nr and χ.

Table 1. Calculated values of skin fricatons $f''(0)$ and $g''(0)$.

			$c = 0$		$c = 0.5$	$c = 1$
M	β	λ	-$\left(1 + \frac{1}{\beta}\right) f''(0)$	-$\left(1 + \frac{1}{\beta}\right) f''(0)$	-$\left(1 + \frac{1}{\beta}\right) g''(0)$	-$\left(1 + \frac{1}{\beta}\right) g''(0)$
0	1000	0	1.00049 [19]	-1.09363 [19]	0.46543 [19]	-1017430 [19]
0	5	0	1.09544	1.19742	0.50960	1.28574
0	1	0	1.41422	1.54587	0.65790	1.65988
0	1	0.5	1.73205	1.83608	0.82283	1.93155
0	1	1	1.99999	2.08845	0.96138	2.17180
10	100000000	0	3.31662 [19]	3.34202 [19]	1.64588 [19]	3.36721 [19]
10	5	0	3.63318	3.66100	1.80297	3.68859
10	1	0	4.69041	4.72634	2.32764	4.76198
10	1	0.5	4.79583	4.83095	2.38072	4.86580
10	1	1	4.89897	4.93334	2.43265	4.96745
100	100000000	0	10.04987 [19]	10.05817 [19]	5.02079 [19]	10.06646 [19]
100	5	0	11.00908	11.01817	5.50000	11.02726
100	1	0	14.21267	14.224397	7.10046	14.23611
100	1	0.5	14.24780	14.25950	7.11804	14.27119
100	1	1	14.28285	14.29452	7.13552	14.30618

TABLE 2. Calculated values of Nusselt number–$\theta'(0)$ and Sherwood number–$\phi'(0)$ for different parameters.

M	Nr	Pr	Nb	Nt	Le	χ	λ	Bi	$-\theta'(0)$	$-\phi'(0)$
0.1	0.1	0.1	0.1	0.1	0.1	0.1	0.1	0.1	0.4143701	0.414370
0.5									0.4143701	0.061632
1.0									0.4143701	0.061632
	0.3								0.3887338	0.034847
	0.5								0.3679027	0.013463
	0.7								0.3504527	0.004169
		1.5							0.3987212	0.045223
		2.0							0.4338778	0.082334
		2.5							0.4614280	0.112004
			0.08						0.4625572	0.112004
			0.06						0.4636843	0.356605
			0.04						0.4648090	0.662346
				0.03					0.4665408	0.026196
				0.05					0.4660475	0.208651
				0.07					0.4655530	0.390549
					0.2				0.4640750	0.220643
					0.3				0.4630327	0.094268
					0.4				0.4622297	0.008461
						0.3			0.4617116	0.109761
						0.5			0.4612668	0.200081
						0.7			0.4608786	0.281824
							0.4		0.4608786	0.281824
							0.7		0.4608786	0.281824
							1.0		0.4608786	0.281824
								1.5	0.5436251	0.206841
								2.0	0.5970751	0.158550
								2.5	0.6344249	0.124873

The effects of magnetic parameter M for each velocity components (f', g') on temperature θ and concentration ϕ profiles are displayed in Figures 2, 3, 4 and 5. For electric conduction to inflict the magnetic parameter M, a drag force or resistive force known as Lorentz force exist. This force has a tendency to slow down the speed of the flowing fluid. Decreasing in the velocity profiles are seemed by increasing the magnetic factor M along the $x-$ and y-direction. The Lorentz force mentioned above affects the magnetic parameter; M works like a proxy in the fluid flow resistance. Also, changing the value M, change is seen in the Lorentz force, and decreasing is seen in both velocity profiles. Also, changing the value of M, we can notice changes in the concentration profile, boundary layer wideness, and species boundary layer. The obtained results clearly show that the magnetic parameter M is in the transverse track with marvels of conveyance. This is the critical remark that the enormous hurdles in the flow of fluid particles cause heat generation. As a result, an increase is noticed when the magnetic field is enlarged. Figures 6 and 7 epitomize the behaviour of non-Newtonian parameter β on the both velocity profiles $f'(\eta)$ and $g'(\eta)$. From figure, it is examined that with increment in β, it yields confrontation in the flow field. So, for higher values of β, the boundary layer wideness and the amount of velocity profiles $f'(\eta)$ and $g'(\eta)$ decreased. Indefinitely, with the increment in non-Newtonian parameter β the recent phenomena condense to Newtonian fluid. From Figure 8, it can observed that for increasing non-Newtonian parameter will increase the concentration profile. Figure 9 shows that the temperature profiles increase as thermal radiation increases, and because the effect of Nr is to enhance heat transfer, the thermal boundary layer thickness increases with thermal

radiation. Figure 10 shows the influence of thermophoresis parameter Nt against the temperature distribution. For large values of Nt, the molecules start movements from hot to the cooler surface. As a result, an improvement is recorded in the boundary layer wideness, which leads to an increase in the temperature profile. The graphical impact of the parameter Le on the concentration of fluid particles is reflected in Figure 11. Le represents the relation between influence of the rate of thermal and species diffusions in the region along the boundary layer. To increase the parameter Le, the boundary layer region involving species are crippled and the temperature profile gets elevated. Figures 12, 13 show the relationship between nanoparticle concentration C, and the velocity profile $f'(\eta)$ and the concentration profile are discussed. By increasing the concentration profile C, the increment in velocity profile along the x-direction is shown in the figure, whereas the opposite behaviour is shown in the concentration profile, i.e., by increasing the nano-particle concentration C, the concentration profile decreased. Figure 14 provides the influence of chemical reaction factor on concentration profile. By increasing the chemical reaction factor, decrement is exposed in the concentration profile. Figures 15, 16, 17, 18 elucidates the influence of porosity parameter on velocitie, temperature and concentration profiles. From graphs it is seen that for increasing values of porosity parameter λ, the velocities in the boundary layer decrease in both directions. The presence of porous media creates huge resistance to fluid flow due to which there occur insignificant changes in the momentum boundary layer and hence there appears provocative for the fluid temperature. Moreover, the boundary layer thickness also decreases for higher values of λ, whereas opposite trend is noted for temperature and concentration profiles.

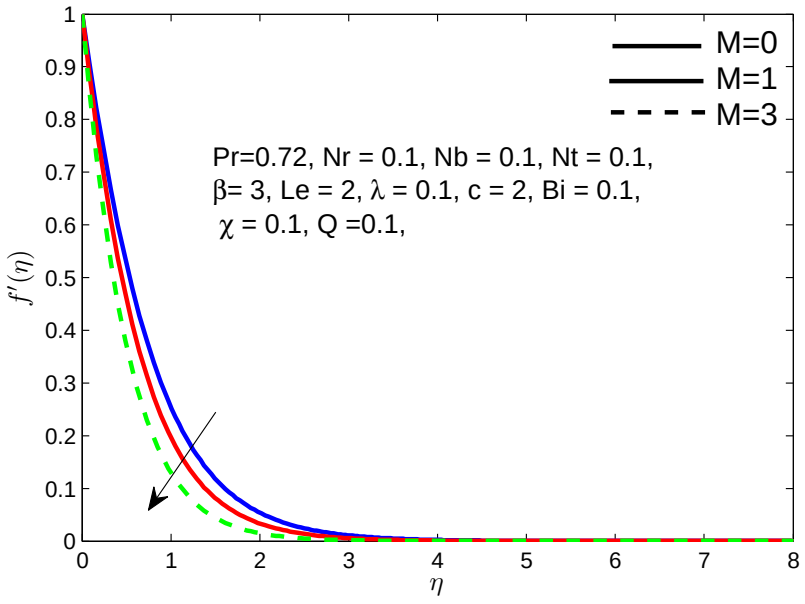

FIGURE 2. Inspiration of M on $f'(\eta)$.

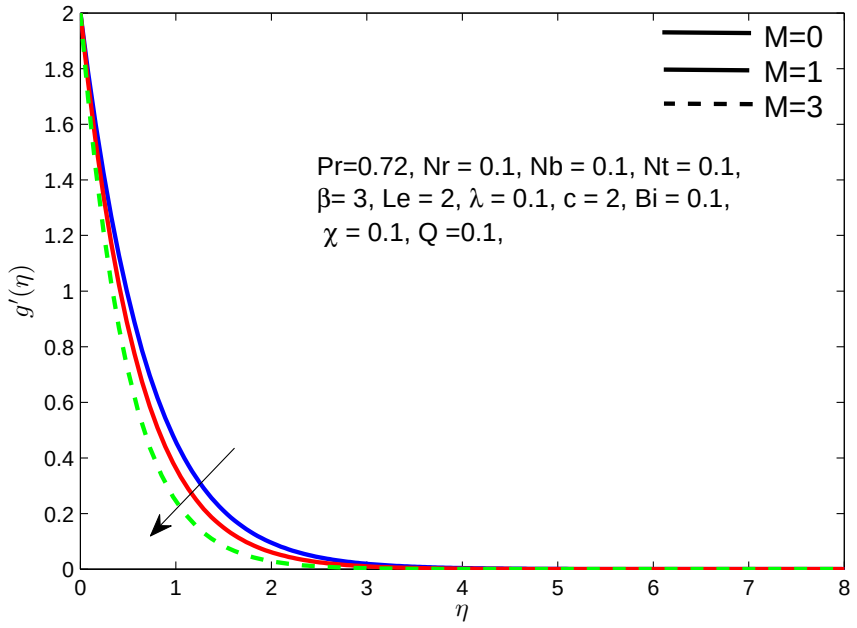

FIGURE 3. Inspiration of M on $g'(\eta)$.

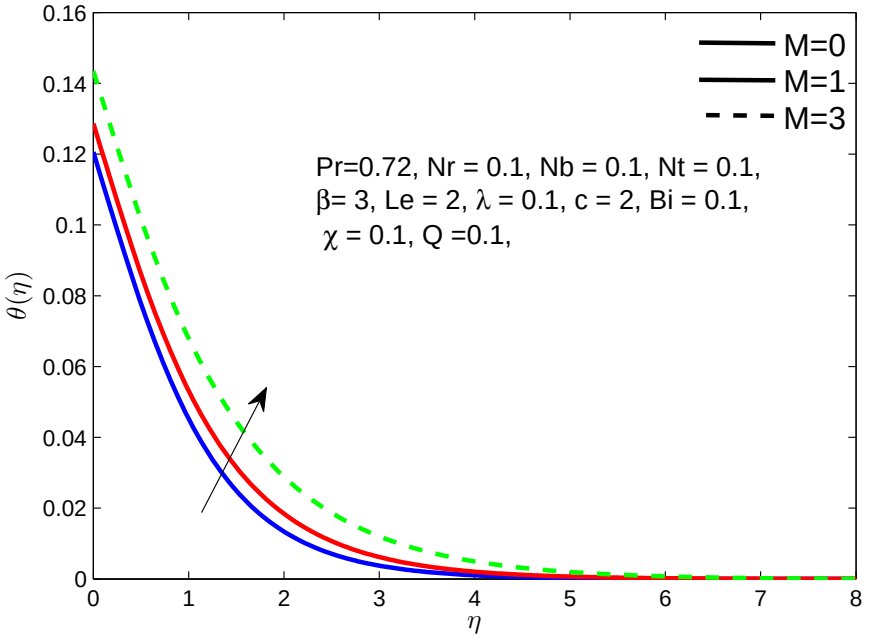

FIGURE 4. Inspiration of M on $\theta(\eta)$.

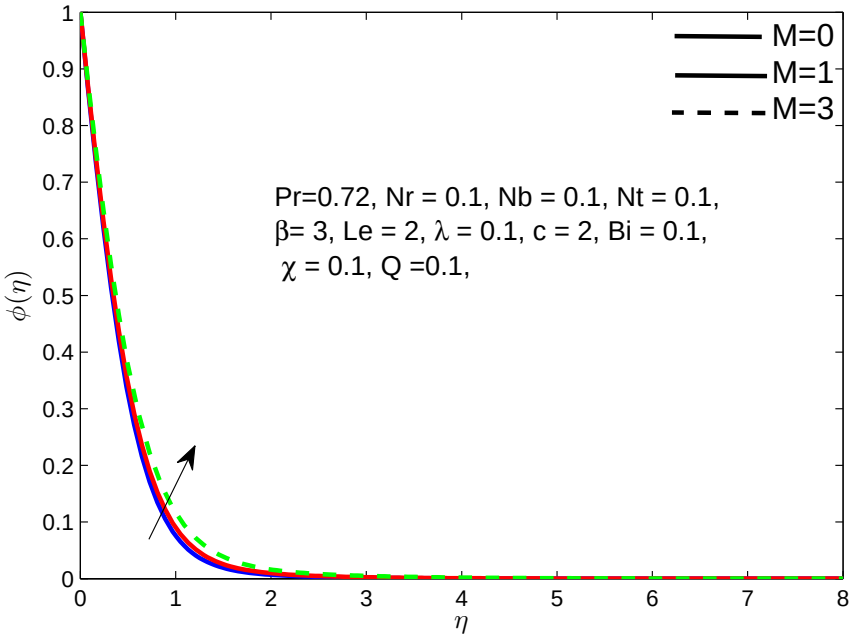

FIGURE 5. Inspiration of M on $\phi(\eta)$.

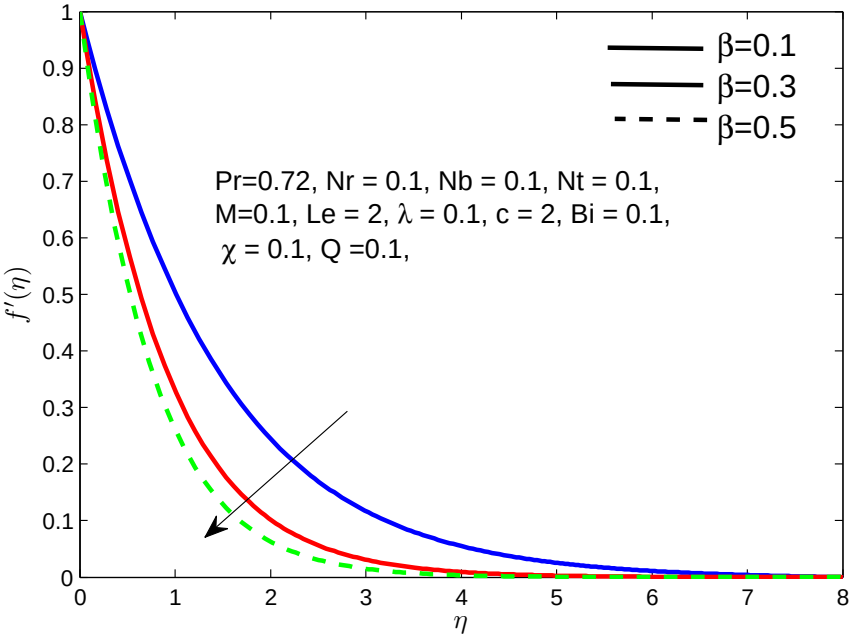

FIGURE 6. Inspiration of β on $f'(\eta)$.

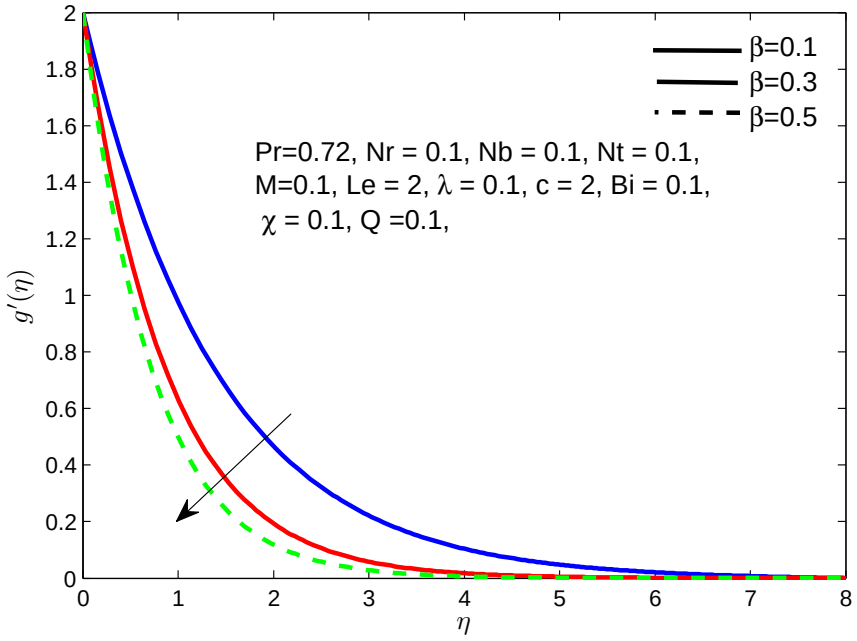

FIGURE 7. Inspiration of β on $g'(\eta)$.

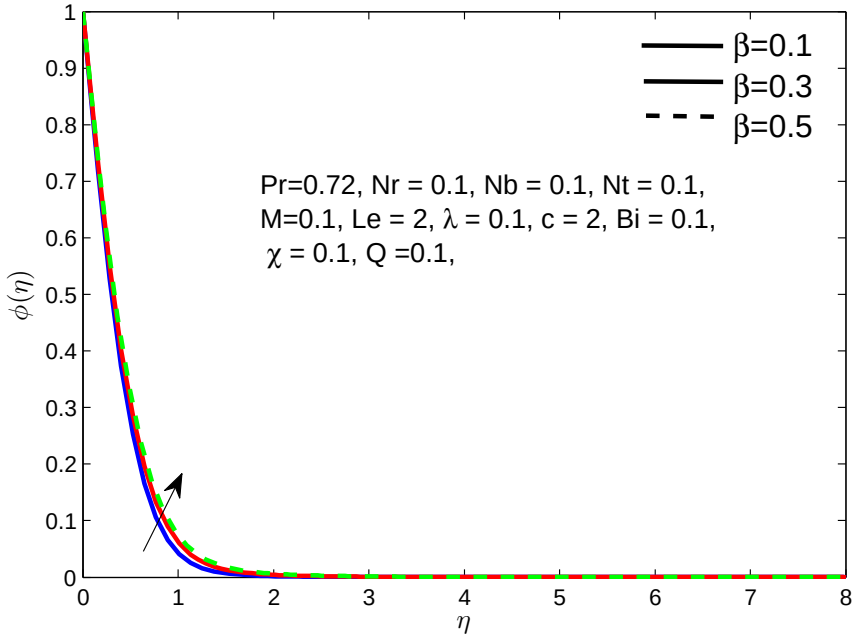

FIGURE 8. Inspiration of β on $\phi(\eta)$.

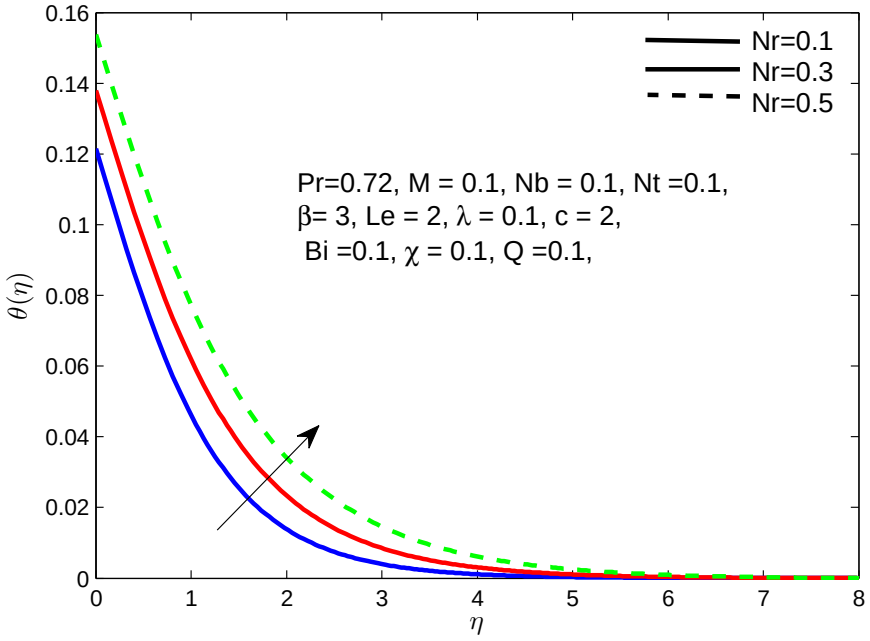

FIGURE 9. Inspiration of Nr on $\theta(\eta)$.

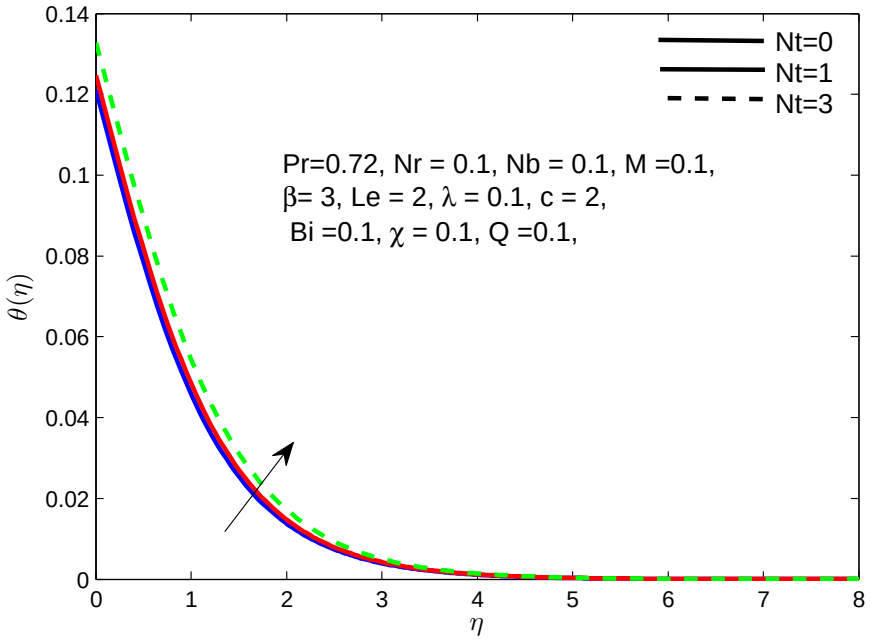

FIGURE 10. Inspiration of Nt on $\theta(\eta)$.

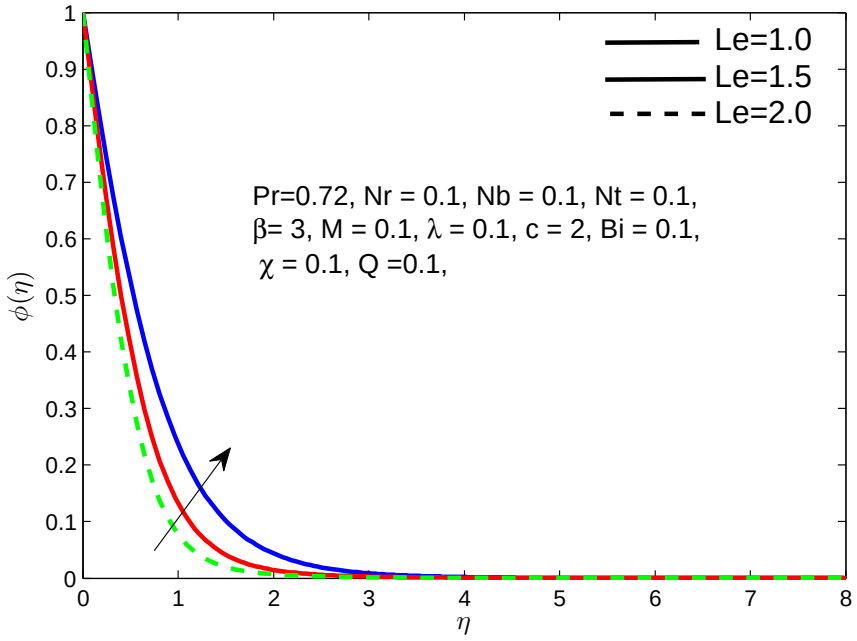

FIGURE 11. Inspiration of Le on $\phi(\eta)$.

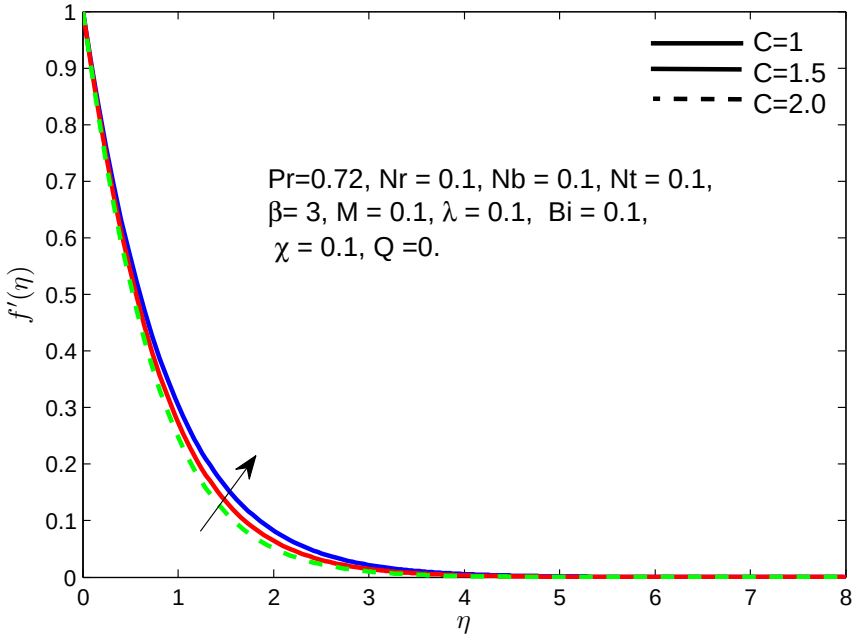

FIGURE 12. Inspiration of C on $f'(\eta)$.

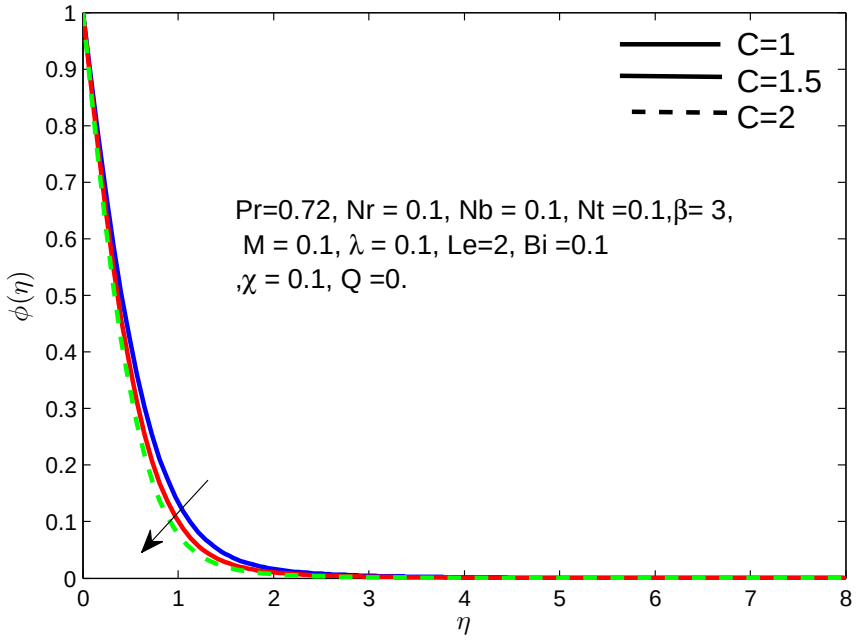

FIGURE 13. Inspiration of C on $\phi(\eta)$.

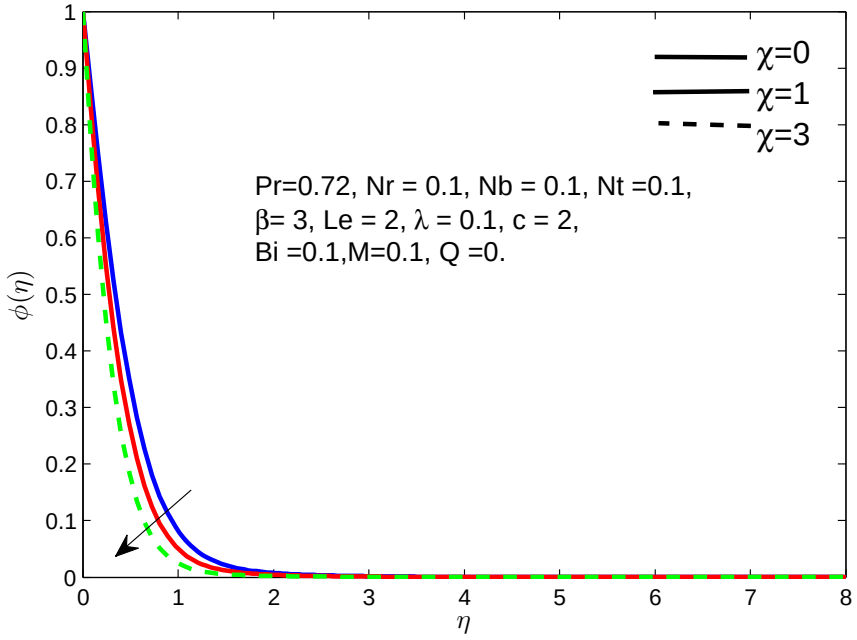

FIGURE 14. Inspiration of χ on $\phi(\eta)$.

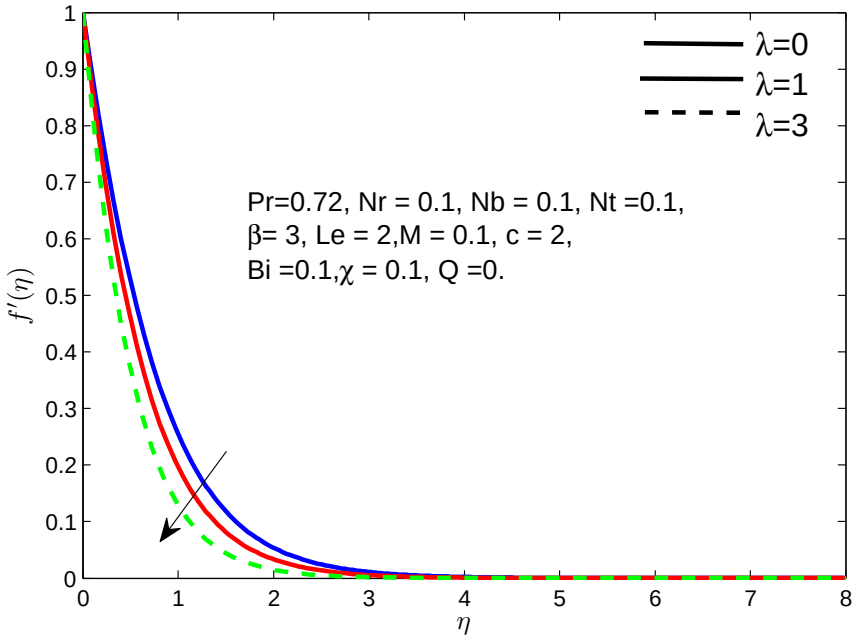

FIGURE 15. Inspiration of λ on $f'(\eta)$.

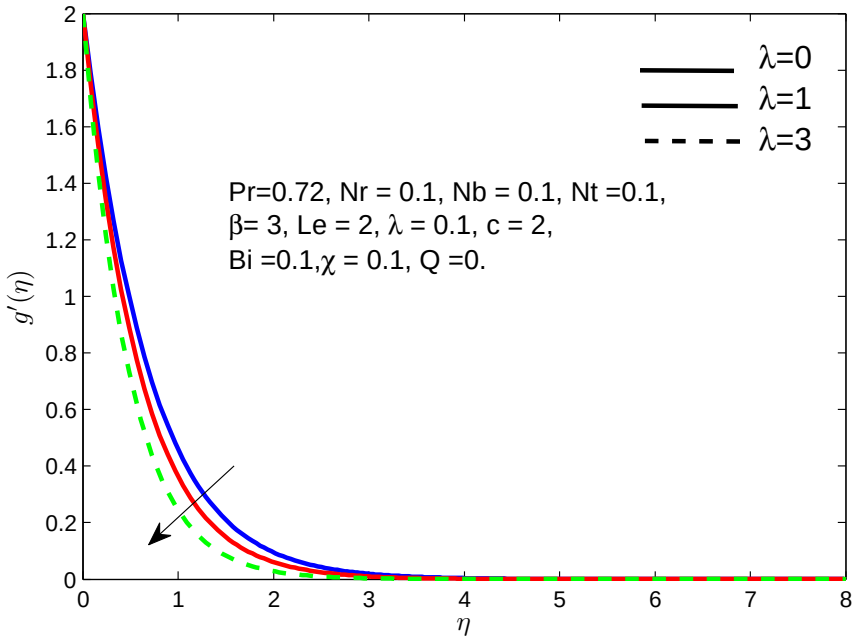

FIGURE 16. Inspiration of λ on $g'(\eta)$.

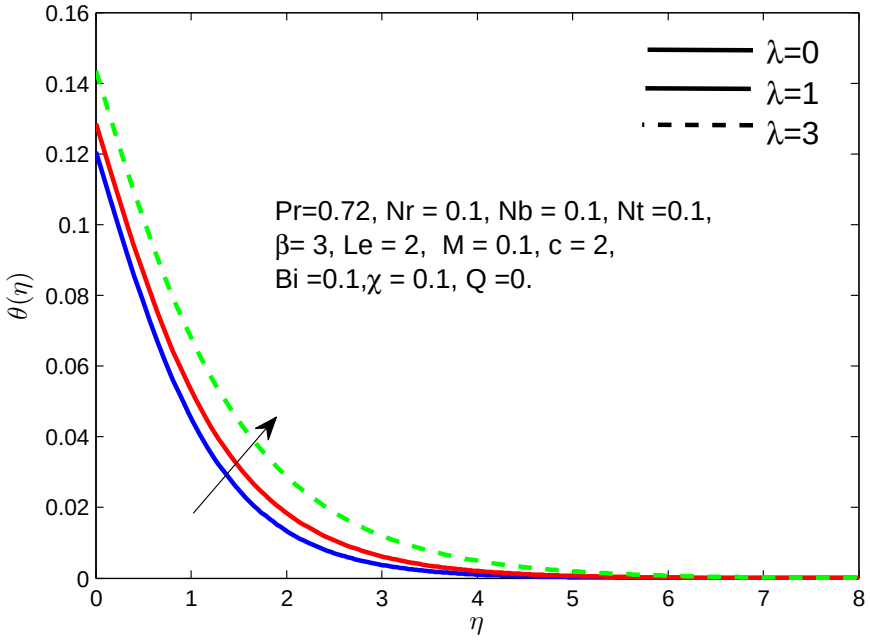

FIGURE 17. Inspiration of λ on $\theta(\eta)$.

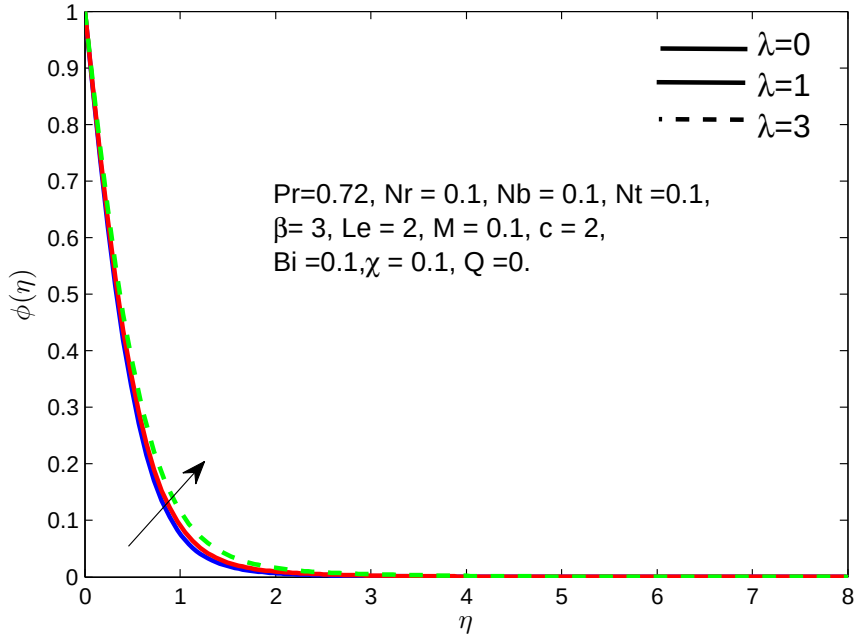

FIGURE 18. Inspiration of λ on $\phi(\eta)$.

5. Conclusion

In the recent article, three-dimensional MHD Casson liquid flow and heat transfer towards a stretched surface with the aid of thermal radiation, Brownian motion, chemical reaction nanoparticle

concentration have been verified pictorially. In addition, the proposed boundary layer equations are solved numerically using MATLAB bvp4c function with shooting technique. The important findings of the present study are outlined as:

- By increasing the magnetic parameter M, the velocity profiles decrease, and for concentration profiles and temperature profiles, the opposite performance has been perceived.
- It is also noticed that the concentration profile reduces by raising the value of Le.
- An increment is noticed in temperature profiles by accelerating the radiation parameter, Nr and thermophoresis parameter Nt.

References

1. H. Baber, H. M Ali, Towards hybrid nanofluids: preparation, thermophysical properties, applications, and challenges. *Journal of Molecular Liquids* **281** (2019), 598–633.
2. S. U. S. Choi, Enhancing Thermal Conductivity of Fluids with Nanoparticles, In: *Developments and Applications of Non-Newtonian Flows* (D. A. Siginer and H. P. Wang, Eds.), vol. 66, pp. 99–105, ASME, New York, 1995.
3. R. Ellahi, Effects of the slip boundary condition on non-Newtonian flows in a channel. *Communications in Nonlinear Science and Numerical Simulations* **14** (2009), no. 4, 1377–1384.
4. R. Ellahi, A. Riaz, Analytical solutions for MHD flow in a third-grade fluid with variable viscosity. *Math. Comput. Modelling* **52** (2010), no. 9-10, 1783–1793.
5. M. H. Esfe, A. Tatar, M. R. H Ahangar, H. Rostamian, A comparison of performance of several artificial intelligence methods for predicting the dynamic viscosity of TiO2/SAE 50 nano-lubricant. *Physica E: Low-dimensional Systems and Nanostructures* **96** (2018), 85–93.
6. N. Freidoonimehr, A. B. Rahimi, Investigation of MHD nano-fluid flow over a stretching surface with velocity slip and convective surface boundary conditions. *Modares Mechanical Engineering* **15** (2015), no. 3, 208–218.
7. M. Goodarzi, M. R. Safaei, K. Vafai, G. Ahmadi, M. Dahari, S. N. Kazi, N. Jomhari, Investigation of nanofluid mixed convection in a shallow cavity using a two-phase mixture model. *International Journal of Thermal Sciences* **75** (2014), 204–220.
8. A. Ishak, R. Nazar, I. Pop, Mixed convection boundary layers in the stagnation-point flow toward a stretching vertical sheet. *Meccanica* **41** (2006), no. 5, 509–518.
9. A. Khalid, I. Khan, S. Shafiq, Exact solutions for unsteady free convection flow of Casson fluid over an oscillating vertical plate with constant wall temperature. In: *Abstract and Applied Analysis*, vol. 2015. Hindawi, 2015.
10. A. A. Khan, S. R. Bukhari, M. Marin, R. Ellahi, Effects of chemical reaction on third-grade MHD fluid flow under the influence of heat and mass transfer with variable reactive index. *Heat Transfer Research* **50** (2019), no. 11, 1061–1080.
11. W. A. Khan, A. Waqar, R. Culham, O. D. Makinde, Hydromagnetic Blasius flow of power-law nanofluids over a convectively heated vertical plate. *The Canadian Journal of Chemical Engineering* **93** (2015), no. 10, 1830–1837.
12. A. Kilicman, Y. Khan, A. Akgul, N. Faraz, E. K. Akgul, M. Inc, Analytic approximate solutions for fluid flow in the presence of heat and mass transfer. *Thermal Science* **22** (2018), no. 1, 259–264.
13. A. Majeed, A. Zeeshan, H. Xu, M. Kashif, U. Masud, Heat transfer analysis of magneto-Eyring–Powell fluid over a nonlinear stretching surface with multiple slip effects: Application of Roseland's heat flux. *Canadian Journal of Physics* **97** (2019), no. 12, 1253–1261.
14. O. D. Makinde, A. Aziz, Boundary layer flow of a nanofluid past a stretching sheet with a convective boundary condition. *International Journal of Thermal Sciences* **50** (2011), no. 7, 1326–1332.
15. A. Malvandi, D. D. Ganji, Mixed convective heat transfer of water/alumina nano-fluid inside a vertical microchannel. *Powder Technology* **263** (2014), 37–44.
16. A. D. Manasrah, I. W. Almanassra, N. N. Marie, U. A. Al-Mubaiyedh, T. Laoui, M. A. Atieh, Surface modification of carbon nanotubes with copper oxide nanoparticles for heat transfer enhancement of nanofluids. *RSC Advances*, **8** (2018), no. 4, 1791–1802.
17. A. M. Megahed, Effect of slip velocity on Casson thin film flow and heat transfer due to unsteady stretching sheet in presence of variable heat flux and viscous dissipation. *Appl. Math. Mech. (English Ed.)* **36** (2015), no. 10, 1273–1284.
18. S. Nadeem, R. Haq, N. S. Akbar, Z. H. Khan, MHD three-dimensional Casson fluid flow past a porous linearly stretching sheet. *Alexandria Engineering Journal* **52** (2013), no. 4, 577–582.
19. S. Nadeem, S. Zaheer, T. Fang, Effects of thermal radiation on the boundary layer flow of a Jeffrey fluid over an exponentially stretching surface. *Numerical Algorithms* **57** (2011), no. 2, 187–205.
20. R. Nazar, N. Amin, D. Filip, I. Pop, Unsteady boundary layer flow in the region of the stagnation point on a stretching sheet. *Internat. J. Engrg. Sci.* **42** (2004), no. 11-12, 1241–1253.
21. M. V. Ochoa, *Analysis of Drilling Fluid Rheology and Tool Joint Effect to Reduce Errors in Hydraulics Calculations*. Texas A&M University, 2006.
22. M. M. Rashidi, N. Freidoonimehr, A. O. A. Hosseini, T. K. Hung, Homotopy simulation of nanofluid dynamics from a non-linearly stretching isothermal permeable sheet with transpiration. *Meccanica* **49** (2014), no. 2, 469–482.
23. M. G. Reddy, Unsteady radiative-convective boundary-layer flow of a Casson fluid with variable thermal conductivity. *Journal of Engineering Physics and Thermophysics* **88** (2015), no. 1, 240–251.

24. S. U. Rehman, A. Zeeshan, A. Majeed, M. B. Arain, Impact of Cattaneo-Christov heat flux model on the flow of Maxwell ferromagnetic liquid along a cold flat plate embedded with two equal magnetic dipoles. *J. Magn* **22** (2017), no. 3, 472–477.
25. T. Saeed, I. Abbas, M. Marin, A GL model on thermo-elastic interaction in a poroelastic material using finite element method. *Symmetry* **12** (2020), no. 3, 488.
26. M. Sheikholeslami, D. D. Ganji, Heat transfer of Cu-water nanofluid flow between parallel plates. *Powder Technology* **235** (2013), 873–879.
27. R. Tian, X. Dai, D. Wang, L. Shi, Study of variable turbulent Prandtl number model for heat transfer to supercritical fluids in vertical tubes. *Journal of Thermal Science* **27** (2018), no. 3, 213–222.

(Received 17.05.2021)

[1]Department of Mathematics, The University of Faisalabad, Sargodha Road, University Town Faisalabad, 38000, Pakistan

[2]Department of Mathematics and Statistics, FBAS, International Islamic University Islamabad, H-10, Islamabad, 44000, Pakistan

[3]Department of Mathematics and Statistics, Bacha Khan University, Charsadda, 24420, KPK, Pakistan

[4]Department of Informatics, Faculty of Mathematics and Natural Sciences, University of Oslo, Oslo, Norway

E-mail address: mjaaqib@gmail.com; aaqib.majeed@riphahfsd.edu.pk